Cis-Regulatory Editing of Peptide Signaling Rewires Plant Growth-Defense Balance

Authors

Jin C.-Y. Liao[1], Anne-Maarit Bågman[2,3], Angie Liu[1], Yejin Shim[1], Siobhán M. Brady[2,3] and Pamela C. Ronald[1,3,4]

Affiliations

[1]Department of Plant Pathology, University of California, Davis, CA, USA

[2]Department of Plant Biology, University of California, Davis, CA, USA

[3]Genome Center, University of California, Davis, CA, USA

[4]Innovative Genomics Institute, University of California, Berkeley, CA, USA

Abstract

Precise *cis*-regulatory control of gene expression is essential for balancing plant growth and stress responses. In *Arabidopsis thaliana*, PLANT PEPTIDE CONTAINING SULFATED TYROSINE (PSY) peptides and their receptors (PSYRs) mediate growth–stress trade-offs, yet the transcriptional regulation of these genes remains poorly understood. Here, we mapped transcription factor (TF)–promoter interactions for nine *PSY* and three *PSYR* genes by combining high-throughput yeast one-hybrid screening with DAP-seq data, uncovering 1,207 interactions that reveal both shared and gene-specific regulatory relationships. Functional analysis of 25 TF mutants identified 12 regulators that significantly influence shoot and root growth, most acting as repressors. Of these, CYTOKININ RESPONSE FACTOR 10 (CRF10) emerged as a strong growth inhibitor. We found a CRF10 binding motif in the *PSYR3* promoter using DAP-seq data and validated by eY1H. Guided by these insights, we applied CRISPR/Cas9-mediated promoter editing to precisely delete functional TF-binding sites. Removal of this motif, or its surrounding region, reduced *PSYR3* expression and enhanced root growth, yielding variants that retained root length comparable to the *crf10* mutant but displayed reduced susceptibility to *Pseudomonas syringae* pv. tomato (*Pst*) DC3000. Together, our results define the global TF–promoter interaction network of the *PSYR/PSY* pathway and identify CRF10 as a key transcriptional regulator of *PSYR3*-mediated signaling. More broadly, our work demonstrates that *cis*-regulatory editing can systematically fine-tune gene expression, generate predictable growth traits, and provide a TFBS-targeted framework for engineering plant growth–defense balance.

Introduction

Plants continuously face the fundamental challenge of balancing growth and defense, two competing physiological priorities essential for survival and reproduction. Growth maximizes biomass accumulation and competitive ability, while defense mechanisms protect against pathogens and herbivores. This trade-off is tightly regulated by complex signaling networks that integrate environmental cues with internal developmental programs. Small secreted peptides have emerged as pivotal regulators in this process. The PLANT PEPTIDE CONTAINING SULFATED TYROSINE (PSY) family and their receptors (PSYRs) form a conserved signaling module in *Arabidopsis thaliana* that modulates cell expansion, root development, and stress responses[1–5]. PSY peptides promote growth by stimulating cell elongation and division while interfacing with defense pathways to fine-tune resource allocation under stress. Despite their importance, the transcriptional mechanisms controlling *PSYR* and *PSY* gene expression remain poorly defined, limiting insight into how peptide signaling adapts dynamically to environmental and developmental cues. *Cis*-regulatory elements in gene promoters serve as binding platforms for transcription factors (TFs) that orchestrate gene expression spatially and temporally, but integrating high-throughput TF-promoter interaction data into functional regulatory modules remains challenging. Precise manipulation of such *cis*-elements for trait engineering is further complicated by redundancy and incomplete functional annotation.

CRISPR/Cas-mediated promoter and *cis*-regulatory element (CRE) editing provides powerful tools to fine-tune gene expression and optimize crop traits. Approaches include multiplexed promoter targeting, CRE disruption or deletion, and promoter insertion or swapping[6]. Multiplexed CRISPR/Cas tiling screens in tomato, maize, and rice have demonstrated the potential of systematic CRE editing, although large-scale identification of functional elements remains limited[7–9]. Targeted CRE disruption has enhanced stress responses and disease resistance. In rice, editing the GT-1 element ('GAAAAA') in the *Oryza sativa RAV2* (*OsRAV2*) promoter modulated salt tolerance[10], while deletion of a TALe (Transcription Activator-Like effector)-binding element in the *SWEET11*, a sugar transporter gene, promoter improved bacterial blight resistance without affecting fertility[11–13]. Similarly, mutations in barley's *Hordeum vulgare* purple acid phosphatase a (*HvPAPhy_a*) promoter reduced phytase activity[14], and disruption of Lateral Organ Boundaries 1 (LOB1) promoter elements in citrus conferred canker resistance[15–17]. CRE editing in introns or downstream regions further expands versatility, as shown by gain-of-function *Solanum lycopersicum* WUSCHEL (*SlWUS*) alleles in tomato[7,18]. Beyond plants, CRISPR-mediated disruption of transcription factor binding sites has been demonstrated in human cells and preclinical models[19]. In crops, understanding transcriptional networks that regulate growth-defense trade-offs, where activating defense often limits growth, will be critical for engineering resilient plants with optimized productivity. Promoter editing research has produced promising examples; however, tiling-deletion-based screens remain labor- and time-intensive, as they require analysis of numerous edited variants. Moreover, no gene regulatory network (GRN)-guided approach currently allows for precise, minimal modifications with predictive insight into the functional consequences of promoter elements, limiting the scalability of promoter editing.

Here, we integrated high-throughput enhanced yeast one-hybrid (eY1H) screening of nine *PSY* and three *PSYR* promoters with DAP-seq data to generate a comprehensive TF–promoter interaction network comprising over 1,200 interactions. Functional validation of selected TFs through loss-of-function mutants and overexpression lines identified regulators modulating *PSYR/PSY* expression and growth phenotypes. Informed by this network, we implemented a CRISPR/Cas9-based promoter editing strategy to precisely delete selected transcription factor binding sites, enabling targeted modulation of *PSYR/PSY* expression. This work establishes a framework for mapping and manipulating transcriptional control of peptide signaling pathways, demonstrating how promoter editing can optimize growth–defense trade-offs with high precision.

Results

Mapping the *PSYR*/*PSY* transcriptional regulatory network

To investigate transcriptional regulation underlying PSY peptide signaling, we performed eY1H assays on three *PSYR* and nine *PSY* promoters using a curated *Arabidopsis* transcription factor (TF) library. Integration with publicly available DAP-seq datasets[20] identified 1,207 TF–promoter interactions, with 50–160 binding events per promoter. Approximately 2,000 TFs were screened via eY1H, while ~500 TFs were assessed using the Arabidopsis mesophyll cell DAP-seq dataset. These interactions revealed both shared and gene-specific regulatory relationships across the *PSYR*/*PSY* family, forming a comprehensive transcriptional map of PSY perception and peptide transcription (Fig. 1 and Dataset S1). Network analysis further uncovered clusters of TFs potentially coordinating growth and defense responses, and several central hubs emerged as candidate regulators for functional validation. eY1H assays capture promoter–TF interactions in yeast that often reflect regulatory relationships *in planta*, whereas DAP-seq provides direct evidence of TF–promoter binding sites. Integration of both datasets revealed limited overlap between the two methods. Specifically, three TFs were identified for the *PSYR1* promoter, eight for *PSYR2*, six for *PSYR3*, sixteen for *PSY1*, four for *PSY2*, two for *PSY3*, seven for *PSY4*, one for *PSY5–8*, and three for *PSY9* (Fig. S1 and Dataset S2). Together, these shared interactions highlight a small but robust set of candidate regulators supported by both approaches.

To understand how these regulatory interactions manifest *in planta*, we next examined gene expression patterns across tissues and cell types. Complementary analyses from publicly available RNA-seq datasets defined the expression patterns of *PSYR* and *PSY* genes across *Arabidopsis* tissues. All three *PSYR*s were broadly expressed, with *PSYR1* enriched in shoots and *PSYR3* in roots (Fig. S2a). Among the peptides, *PSY1* was the most abundant and widely expressed, whereas *PSY7* showed minimal expression. *PSY4* was localized to root tips and shoot apices, and *PSY9* was primarily expressed in reproductive tissues (Fig. S2b). Single-cell data from the Plant sc-Atlas[21] further revealed cell-type specificity. *PSY3* and *PSY4* co-localized in root cell types, suggesting overlapping functions, while *PSY6* and *PSY8* displayed distinct but complementary root-specific patterns (Fig. S3). Together, these findings underscore the importance of spatial regulation and receptor–ligand interplay in shaping root system architecture (RSA) phenotypes.

To link these interactions to functional outputs, we integrated interaction data with expression profiles. This co-expression analysis identified numerous candidate TFs with potential roles in modulating PSY perception and peptide expression, highlighting a complex transcriptional architecture (Fig. S4). The network is organized around a small set of highly connected TF hubs, providing testable entry points for dissecting how transcriptional programs coordinate PSY signaling with developmental and stress-responsive processes.

Network-guided selection and screening of TFs for promoter editing

To identify precise promoter editing sites for predictive phenotypic outcomes, we systematically dissected transcription factor binding sites across all 3 *PSYR* and 9 *PSY* promoters using the mapped TF–promoter interactions. Focusing on root system architecture (RSA) as a readout, given its sensitivity to subtle promoter changes and the availability of high-throughput phenotyping tools, we developed a workflow that integrates transcription factor binding sites mapping with functional assays to prioritize regulatory regions for CRISPR-based editing (Fig. 2a). Candidate TFs were identified by combining whole-promoter interaction assays (eY1H) with DAP-seq data. Although a root-specific DAP-seq dataset would be ideal, it is not currently available. By prioritizing TFs identified in both approaches, we obtained 40 high-confidence candidates, from which 12 with available homozygous mutant lines and an additional 10 detected only by DAP-seq (represented by 13 independent homozygous alleles) were selected for phenotypic analysis (Dataset S2, S3, and Table S2).

Phenotypic analysis revealed that mutants of the 12 TFs identified by both eY1H and DAP-seq exhibited significant changes in at least one RSA trait. Ten alleles displayed increased primary root length (*crf10*, *tga2 tga5*, *wrky8-1*, *myb77-2*, *myb73-1*, *hb34*, *myb70-2*, *at3g42860*, *abi5-10*, *wrky14*), while two showed no change (*rap2.11*, *atrav1.1*) (Fig. 2b-d). Among the DAP-seq-only TFs, 6 alleles displayed increased root length (*wrky22-1*, *wrky22-2*, *wrky22-3*, *anac087-2*, *erf11*, *aif*), one allele decreased (*ein3-1*), and 7 exhibited no change (*hca2*, *pear2*, *myb3r4-3*, *tga10*, *ntl4-1*, *erf4-1*, *ntl8-1*) (Fig. S6). Many of these alleles had been studied previously, but root phenotypes were largely unreported or poorly described, with *myb70-2* as the only clearly documented case[22], showing a longer primary root consistent with our observations. Overall, 17 mutants exhibited significant changes in shoot or root growth compared with wild-type plants, 16 of which displayed increased biomass and enhanced RSA, suggesting that multiple TFs act as growth repressors to fine-tune the balance between growth and stress responses. Overexpression lines of five TFs, including less-characterized candidates, most of which exhibited stunted growth, further confirmed their function as growth repressors (Fig. S7). Collectively, these results establish a direct link between TF–promoter interactions and *PSYR*/*PSY*-mediated growth regulation, providing an experimentally grounded framework for rational promoter engineering to refine RSA phenotypes.

Tissue-specific transcriptional rewiring in TF knockout lines

To assess whether candidate TFs act as activators or repressors of *PSYR*/*PSY* transcription and whether their regulation is tissue-specific, we measured transcript levels in shoots and roots of selected TF knockout lines using quantitative PCR. Knockouts were first validated by PCR genotyping and qPCR (Fig. S5). To link TF binding with RSA phenotypes, we focused on three *PSYR* and three *PSY* promoters with the highest number of candidate TF interactions. Homozygous TF knockout lines were analyzed, with shoot and root tissues collected separately to capture potential tissue-specific regulation. qRT–PCR analyses revealed consistent alterations in *PSYR* and *PSY* expression, directly connecting TF–promoter interactions to transcriptional outputs.

Most mutants showed altered expression of *PSYR*/*PSY* target genes, with distinct patterns of activation and repression. MYB70 bound the promoters of both *PSYR1* and *PSYR2* and repressed their transcription, whereas MYB73 bound the *PSYR1* promoter but acted in a tissue-specific manner, repressing transcription in shoots while activating it in roots. CRF10 bound the *PSYR3* promoter and activated transcription in both tissues, while TGA5 and WRKY8 each activated *PSY1* transcription. In contrast, ABI5 consistently functioned as a repressor, binding both *PSY1* and *PSY4* promoters and reducing expression in shoots and roots. Finally, RAV2.11 bound the *PSY2* promoter and exerted opposite effects across tissues, activating transcription in shoots while repressing it in roots (Fig. 3 and Data S4). These transcriptional outcomes are consistent with direct TF-mediated regulation, and the magnitude and tissue specificity of expression changes correlated with the growth phenotypes of the corresponding knockout lines, supporting a model in which these TFs fine-tune PSY signaling through spatially resolved transcriptional control. Overall, these results demonstrate that tissue-specific transcriptional rewiring of *PSYR* and *PSY* genes is predictable from large-scale TF–promoter interaction datasets and provide mechanistic evidence that combinatorial TF activity shapes spatial patterns of PSY signaling, ultimately influencing growth and RSA phenotypes.

Precision promoter editing of *PSYR3* reshapes growth and defense

To test whether disruption of transcription factor binding sites could modulate gene expression and plant growth, we implemented a CRISPR/Cas9-based promoter editing strategy. Candidate motifs within *PSYR* and *PSY* promoters were targeted, focusing initially on the *PSYR3* promoter. A putative CRF10 binding motif (‘CGGCGG’) was identified in the *PSYR3* promoter using DAP-seq data and validated by eY1H. CRF10 is a member of the APETALA2 (AP2)/ETHYLENE RESPONSE FACTOR (ERF) transcription factor family, which regulates hormone signaling, stress responses, and development[23]. Although the *Arabidopsis* CRF family contains 12 members, CRF10 remains largely uncharacterized. In Col-0 plants, *CRF10* was expressed ubiquitously, with highest expression in embryos (Fig. S4). In our screening (Fig. 2), *crf10* mutants exhibited longer primary roots and enhanced root system architecture (RSA), whereas overexpression of *CRF10* in wild-type Col-0 caused pronounced growth inhibition, confirming that CRF10 functions as a strong growth repressor (Fig. S7). To directly test whether CRF10 binding influences *PSYR3* expression, we generated CRISPR-edited lines targeting the CRF10 motif in the *PSYR3* promoter. Two guide RNAs were designed

to target both the primary TFBS and adjacent sequences (Fig. 4a). Sequencing of independent lines revealed two distinct alleles. R3pro_Var1 carries a 31 bp deletion immediately adjacent to the DAP-seq–validated CRF10 binding motif, leaving the consensus sequence intact, whereas R3pro_Var2 carries a 27 bp deletion that removes the motif entirely. T2 homozygous lines were used for phenotyping and expression assays.

Phenotypic analysis revealed that promoter-edited plants exhibited altered primary root length compared with wild type, with phenotypes comparable in magnitude to *psyr3-1* and *crf10* knockout mutants (Fig. 4c). Lateral root number remained unchanged (Fig. 4d), but total lateral root length per plant increased (Fig. 4e), resulting in increased total and average lateral root length relative to WT, *psyr3-1*, and *crf10* (Fig. 4f). Both edited alleles also displayed reduced *PSYR3* transcript abundance in the shoot and root relative to wild-type controls (Fig. 4g), with R3pro_Var1 showing reduced expression despite retaining the CRF10 consensus motif, suggesting that sequences adjacent to the motif also contribute to transcriptional regulation.

To examine whether altered RSA affects defense responses, we challenged the edited variants with *Pseudomonas syringae* pv. *tomato* DC3000. We found that *crf10* mutants were more susceptible to infection compared with the WT control. Both promoter-edited variants displayed lower bacterial populations compared with *crf10*, with higher populations compared with WT. Together, these results demonstrate that targeted *cis*-regulatory modification of the *PSYR3* promoter is sufficient to alter gene expression and phenotypic outcomes. These results indicate that CRF10 activates *PSYR3* expression while negatively regulating root system architecture, highlighting the CRF10 transcription factor binding site as a successful target for precision promoter editing to fine-tune gene expression and achieve predictable phenotypic modulation.

Discussion

Our work demonstrates the utility of network-guided promoter editing to fine-tune gene expression through genome editing of transcription factor binding sites. Phenotypic and expression changes in promoter-edited *PSYR3* lines confirm that disrupting predicted regulatory motifs can produce measurable biological outcomes. Notably, altered expression was observed not only when the CRF10 binding motif itself was deleted, but also when nearby promoter regions were perturbed. These results indicate that promoter edits can influence transcriptional activity beyond direct motif removal, emphasizing the importance of local sequence context, motif spacing, DNA structure, and *cis*-regulatory modules in shaping transcriptional output. Even small alterations outside core transcription factor binding sites were sufficient to affect transcription, demonstrating the sensitivity of regulatory networks to local sequence changes. The observation that promoter edits produced phenotypes comparable to gene knockouts illustrates both the promise and complexity of this approach. While transcription factor binding site -level editing allows finer control than complete gene disruption, it also reveals buffering and redundancy inherent in plant regulatory networks. Divergence between *psyr3-1* and *crf10* knockout phenotypes suggests that CRF10 regulates additional downstream targets, while *PSYR3* is likely influenced by multiple transcription factors. These findings highlight that single-site promoter perturbations may only partially recapitulate gene knockout

effects, reflecting the distributed nature of transcriptional control. Together, these results underscore the need to consider promoter architecture, motif spacing, and network connectivity when designing targeted edits, as subtle changes can have wide-ranging effects on transcriptional output.

Beyond mechanistic insights, network-guided promoter editing enables precise, context-aware trait modulation. By selecting functional *cis* elements based on regulatory networks, edits can be designed for tissue-specific or environment-responsive regulation, enhancing trait specificity while minimizing unintended systemic effects. This capability is particularly valuable for complex traits influenced by multiple environmental and developmental cues, where traditional knockout approaches may produce broad pleiotropic effects. Sequences adjacent to transcription factor binding sites contribute significantly to transcriptional output, as even minor alterations can perturb expression. These observations suggest that combinatorial editing of multiple sites within a gene, or across several targets of the same transcription factor, is likely necessary to overcome redundancy and achieve predictable phenotypic outcomes. Such combinatorial strategies can enhance control over quantitative traits and increase the robustness of phenotypic outcomes across different genetic backgrounds and environmental conditions. By integrating tissue- and condition-specific regulatory information, network-guided promoter editing enables the rational design of edits that tune expression in the desired context, offering nuanced control over gene activity. Altogether, these approaches move plant engineering beyond binary knockouts and toward tunable modulation, providing a framework for optimizing traits while preserving overall plant fitness.

Although tiling-deletion-based screens have enabled systematic functional interrogation of regulatory regions, they are labor-intensive, time-consuming, and often less predictive, particularly when applied across multiple genes. Moreover, because these strategies rely on scanning promoter regions through serial deletion or mutagenesis, they tend to reveal functional elements retrospectively rather than enabling targeted modulation. In contrast, our gene regulatory network-guided strategy enables precise selection of functional *cis*-regulatory elements, increasing specificity while reducing experimental complexity. This hypothesis-driven approach facilitates fine-tuning at the gene family level and is compatible with high-throughput, NGS-based genotyping, enabling accurate identification of edited genotypes. By narrowing the range of potential target sites, network-guided editing enhances both predictability and efficiency, laying the groundwork for downstream applications such as base editing or prime editing to precisely tune transcription factor binding sites. Although promoter insertions or swaps remain technically challenging, successful examples, such as the insertion of the *GOS2* promoter upstream of *ARGOS8* in maize to enhance expression and improve drought tolerance[24], demonstrate the potential for context-aware regulatory engineering and create opportunities for synthetic promoter applications by replacing native promoters.

Promoter editing in Arabidopsis remains largely unexplored, yet the species offers rich genomic and regulatory resources, including well-characterized gene regulatory networks, TFBS maps, and promoter motifs. Comparative analyses between Arabidopsis and crop species will be essential to translate these insights to agricultural contexts. While gene regulatory networks are extensively mapped in Arabidopsis, coverage in major crops remains limited. Systematic comparisons of TFBSs, promoter architectures, and

regulatory modules can identify conserved elements, enabling rational design of network-guided promoter edits in crop species. Integrating comparative genomics with functional validation in crops will allow predictions from Arabidopsis to inform trait optimization strategies, including stress resilience, yield improvement, and adaptation to fluctuating environmental conditions. By leveraging evolutionary conservation and incorporating species-specific regulatory data, network-guided editing can bridge the gap between model systems and practical agricultural applications, providing a roadmap for translational *cis*-regulatory engineering.

Future studies will explore how promoter edits impact local chromatin accessibility and higher-order regulatory architecture. Integrating ATAC-seq or other chromatin profiling approaches in edited lines will provide deeper insight into the epigenomic consequences of TFBS-level perturbations and help refine predictive models of *cis*-regulatory engineering. Beyond chromatin accessibility, advanced chromatin conformation capture techniques, such as Hi-C, and super-resolution microscopy will enable mapping of long-range chromatin interactions and three-dimensional promoter-enhancer organization. These approaches will reveal how network-guided promoter edits influence not only local accessibility but also broader regulatory networks. Collaborative integration of epigenomic and imaging data will facilitate comprehensive models linking *cis*-regulatory perturbations to transcriptional and phenotypic outcomes. Extending these analyses across tissues and environmental conditions will further enhance the ability to design edits that achieve context-specific gene regulation while minimizing unintended effects. Additionally, expanding this strategy to include base editing, prime editing, and combinatorial promoter modifications will increase the precision and versatility of *cis*-regulatory engineering. Collectively, these approaches will accelerate the development of crops with optimized traits, improved stress resilience, and enhanced performance across diverse environments.

Methods

Promoter cloning for eY1H.

PSYR and *PSY* gene promoters previously tested in Ogawa-Ohnishi et al.[1] were cloned (Supplementary Table #) using the method described by Gaudinier et al.[25]. Promoters were amplified by PCR from *Arabidopsis thaliana* Col-0 genomic DNA using Phusion High-Fidelity DNA Polymerase (NEB). The amplified promoter fragments were first cloned into the pENTR 5'TOPO vector using the pENTR 5'TOPO kit (Invitrogen) and fully sequenced. Subsequently, promoters were recombined with the Gateway LR reaction into both pMW2 and pMW3[26] Gateway destination vectors (designed for yeast expression and containing respectively *HIS3* or *LacZ* reporter genes) using LR Clonase™ II (Invitrogen). The resulting constructs were sent to Azenta Life Sciences (South Plainfield, NJ, USA; formerly GeneWiz) for whole plasmid sequencing using the Plasmid-EZ nanopore-based sequencing method.

Enhanced Yeast One Hybrid (eY1H) Assay.

Assays were performed according to Gaudinier et al.[25,27]. *PSYR* and *PSY* promoter – pMW2/pMW3 reporter constructs were transformed into yeast strain YM4271. Resulting yeast colonies were screened for autoactivation for both histidine biosynthesis and lacZ activity, and the construct presence within the yeast genome was confirmed by PCR-based genotyping. The resulting bait yeast strains were screened against a complete collection of 2000 Arabidopsis transcription factors[28] in a mating-based assay, and positive interactions were identified for both histidine and lacZ activity compared to a negative control pDESTAD-2μ. An interaction was recorded as successful if there was activation of either HIS or lacZ. The eY1H Yeast One-Hybrid screening was carried out by the Yeast One Hybrid Services Core at the UC Davis Genome Center, at the University of California, Davis. The table with all the results can be found at https://github.com/jcyliao/Liao2025.

Network construction.

Networks were made using Cytoscape v.3.10.2[29]. All cytoscape network files can be found at https://github.com/jcyliao/Liao2025.

DAP-seq data comparison and mutant lines selection.

DAP-seq TF binding data generated by O'Malley et al.[20] were used to identify direct TF–promoter interactions. DAP-seq target genes (fraction of reads in peaks [FRiP] ≥ 5%) for 529 TFs were downloaded from the Plant Cistrome Database. TFs binding to each individual *PSYR*/*PSY* promoter were extracted from the DAP-seq data (Dataset S1). A Python script was then used to compare the TF lists for each promoter from eY1H and DAP-seq experiments, generating lists of overlapping TFs identified by both assays (Dataset S2).

From these comparisons, 40 overlapping TFs and ~20 TFs identified only in DAP-seq were selected based on the availability of loss-of-function mutants. Mutant lines previously used in published studies were prioritized (Table S2).

Expression analysis of *PSYR*/*PSY* genes and their regulatory TFs.

Expression patterns of *PSYR* and *PSY* genes, along with their selected potential regulatory transcription factors (TFs) identified from eY1H and DAP-seq, were analyzed using publicly available datasets. Bulk RNA-seq datasets were collected to examine gene expression across different tissues and developmental stages. Single-cell RNA-seq datasets, including root cell type-specific profiles from the Plant sc-Atlas database[21], were used to assess cell type-specific expression. In addition, MERFISH (Multiplexed Error-Robust Fluorescence In Situ Hybridization) datasets, which provide spatially resolved single-cell expression, were included from 12-day-old seedlings and 30-day-old rosettes infected with *Pseudomonas syringae* pv. *tomato* DC3000 (*Pst* DC3000)[30,31]. Comparative analyses were performed to identify co-expression patterns and potential tissue- or cell type-specific regulatory relationships.

382

383 **Plant materials and growth conditions.**

384 All transgenic lines were generated in the *Arabidopsis thaliana* Col-0 accession, except
385 for *abi5-1*, which was in the Ws-2 background. Loss-of-function TF mutants were obtained
386 from the Arabidopsis Biological Resource Center (ABRC) at Ohio State University. All
387 mutant lines, including those carrying T-DNA insertions, fast neutron-induced mutations,
388 or EMS-induced mutations, were genotyped to confirm homozygosity. Quantitative RT-
389 PCR (qRT-PCR) was performed to verify transcript-level alterations (Fig. S5 and Data S4).
390 The primers used for genotyping and qRT-PCR, along with accession numbers and
391 additional details on the analyzed mutant lines, are provided in Supplementary Table 2.
392 Plants were grown under a 16-hour light/8-hour dark photoperiod for propagation.

393

394 **Generation of TF overexpressing transgenic plants.**

395 The coding sequences for each TF used in this study were obtained from the TF ENTR
396 clone collection[28] and subsequently cloned into the N-GFP tag pGWB506 (Addgene
397 #74848) destination vector using LR Clonase™ II (Invitrogen) for overexpression in plants.
398 The resulting GFP-TF constructs, driven by the 35S promoter, were introduced into
399 *Agrobacterium tumefaciens* strain GV3101 and used to transform *A. thaliana* (Col-0) via
400 the floral dip method[32]. Transgenic lines were selected on ½ MS solid medium
401 supplemented with 25 mg/L hygromycin. Transgene expression was assessed through
402 GFP fluorescence microscopy, PCR, and qRT-PCR. T3 homozygous plants were used
403 for subsequent phenotypic analyses. The primers used for genotyping and accession
404 numbers and additional details on the constructs, are provided in Supplementary Table 1.

405

406 **Plant phenotype analysis of the TF mutants.**

407 Homozygous TF loss-of-function mutants, TF overexpression T3 plants, and the wild-type
408 (WT) controls seeds were sterilized with 25% (v/v) bleach for 20 min, followed by 5
409 washes with sterile Milli-Q water. Sterilized seeds were plated on ½ MS medium
410 supplemented with 1% sucrose and 0.6% Gelzan, then stratified at 4°C for 2–3 days
411 before being transferred to a growth chamber under long-day (LD) conditions (16 h light/8
412 h dark) with 50–60% humidity at 22°C. Mutant lines and wild-type controls were arranged
413 in a randomized block design within the growth chamber. Plate images were scanned at
414 10 days post-germination (10 dpg) using an Epson Expression 12000XL scanner at 300
415 dpi resolution. Root traits were measured from the scanned images, with at least 20 plants
416 per genotype included in each experimental replicate. For root trait measurements,
417 RootNav 1.0[33] was used for image analysis and data extraction. Traits measured included
418 primary root length (PRL), lateral root number (LR) and lateral root length (LRL).
419 Composite traits were analyzed, including total root length (TRL = PRL + LRL), average
420 lateral root length (ALRL = LRL/LR), lateral root density (LRD = LR/PRL), and the
421 percentage of LRL contributing to TRL (LRL/TRL). Variation across these mutants relative
422 to WT was assessed using one-way ANOVA for all RSA traits. Statistical analyses were
423 performed in Python, with significance determined by Tukey's HSD test.

424

425 **RNA extraction and quantitative PCR.**

426 The whole root and shoot parts of 10-day-old seedlings were collected separately. For
427 one shoot sample, shoots from 10 seedlings grown on the same plate were pooled
428 together. For one root sample, roots from 30 seedlings grown on the same plate were
429 pooled together. Three independent replicates per genotype were collected. Total RNA
430 was extracted using TRIzol reagent (Invitrogen) for TF mutant screening experiments and
431 using the RNeasy Plant Mini Kit (QIAGEN) for promoter-edited line experiments, following
432 the manufacturer's instructions. Genomic DNA contamination was removed by RNase-
433 free DNase treatment during RNA extraction, according to the manufacturer's protocols.
434 First-strand cDNA was synthesized using the SuperScript™ III First-Strand Synthesis
435 System for RT-PCR (Invitrogen) following the manufacturer's instructions. Quantitative
436 real-time PCR (qRT-PCR) was performed using iTaq™ Universal SYBR Green Supermix
437 (Bio-Rad) on a Bio-Rad CFX96 Real-Time System coupled with a C1000 Thermal Cycler
438 (Bio-Rad) under the following conditions: initial denaturation at 95°C for 30 s, followed by
439 39 cycles of PCR (denaturation at 95°C for 5 s, annealing at 60°C for 30 s, and extension
440 at 72°C for 20 s). Relative gene expression was determined using the $2^{-\Delta\Delta CT}$ method, with
441 ACTIN2 as the endogenous control. The primers used for qPCR are provided in
442 Supplementary Table 1.

443

444 **Generation of CRISPR/Cas9 promoter editing constructs and plant screening**

445 To precisely modulate transcription factor (TF) binding at the *PSY* and *PSYR* gene
446 promoters, we employed a targeted promoter editing approach using CRISPR/Cas9. This
447 strategy enables deletion or mutation of specific TF binding sites (TFBSs) to disrupt
448 repressive *cis*-regulatory elements and fine-tune gene expression. Promoter regions
449 containing characterized TFBSs were selected based on TF–promoter interaction
450 mapping and mutant phenotypes. Guide RNAs (gRNAs) were designed to flank these
451 sites, and corresponding CRISPR/Cas9 constructs were generated using standard
452 cloning protocols.

453 For the generation of pJL-AtU6.26-gPSYR3-S1S2 entry clone, an EcoRI–AtU6-26
454 promoter–partial pQZ435–BsaI gBlock was synthesized via the IDT gBlock service.
455 gRNAs were designed using CHOPCHOP[34]. , and PTG assembly into pQZ435, with the
456 OsU3 promoter removed, was performed following Xie et al.[35] with minor modifications.
457 The entry clone was transferred into the pRU294 destination vector via Gateway LR
458 recombination, following the manufacturer's instructions, and the resulting construct was
459 transformed into *Agrobacterium tumefaciens* GV3101 for plant transformation. Constructs
460 were transformed into *Arabidopsis thaliana* via Agrobacterium-mediated floral dipping.
461 Rapid screening of Cas9-containing and Cas9-free lines in both T1 and T2 generations
462 was conducted using a seed coat fluorescence marker[36]. Transgenic plants were
463 confirmed by PCR and Sanger sequencing to confirm precise edits disrupting TFBSs.
464 Successfully edited lines were propagated for subsequent phenotypic and gene
465 expression analyses.

Bacterial pathogen growth and infiltration

Ten-day-old seedlings were transferred to soil and grown at 22 °C with 75% humidity and a light intensity of 180 μmol m^{-2} s^{-1} under short-day conditions (9 h light / 15 h dark) in a growth chamber. Plants were used for pathogen infiltration after an additional three weeks. *Pseudomonas syringae* pv. *tomato* (*Pst*) DC3000 carrying a vector control was cultured on King's B medium plates containing antibiotics (kanamycin and rifampicin) at 28 °C for 3 days prior to use.

Bacterial accumulation assays were carried out according to the method of Katagiri et al.[37], with minor modifications. Briefly, *Pst* DC3000 was scraped from plates, resuspended in 10 mM $MgCl_2$, and diluted to an OD600 of 0.001 (approximately 5×10^5 CFU/mL). Leaves were infiltrated on the abaxial side using a 1 mL needleless syringe (2-3 mature leaves per plant, 6-10 plants per treatment) and covered with a transparent dome overnight. Leaf discs (7 mm diameter; 8-10 per sample, three replicates per treatment) were collected at designated time points, ground in 0.5 mL 10 mM $MgCl_2$, and the volume adjusted to 100 μL per disc. Samples were serially diluted (10-fold, 5-6 dilutions), and 10 μL of each dilution was plated on gridded King's B medium plates containing antibiotics (kanamycin and rifampicin). Colonies were counted to calculate CFU per leaf disc, and statistical significance was evaluated using one-way ANOVA followed by Tukey's HSD test.

Figure preparation and statistical analysis

Python was used for statistical analyses and to generate plots. Figures were assembled in Adobe Illustrator. Some illustrations in the workflow (Fig. 2a) were created using BioRender.

Data availability

All supplementary datasets, Cytoscape files, and Python code are available at https://github.com/jcyliao/Liao2025.

Acknowledgements

We thank Bhanu Upadhyayula, Kai Deshpande, and Maya Ziebarth for assistance with organizing genetic materials and performing genotyping experiments. We are also grateful to Valley Stewart for suggestions on bacterial assays and encouragement, and to Qiong Zhang for providing the pQZ435 vector and the modified PTG cloning protocol. This work was supported by the Chan Zuckerberg Initiative and NIH MIRA grant #R35 GM148173 to P.C.R.

Author contributions

J.C.-Y.L. conceived the project, designed the experiments, and conducted most of the experiments and all data analysis. A.B. and the Yeast One-Hybrid (Y1H) Services Core conducted all eY1H screenings. J.C.-Y.L. and A.L. prepared samples for the gene expression assays. A.L. performed most of the root phenotyping raw data acquisition and, together with Y.S., carried out qPCR measurements. Both A.L. and Y.S. participated in mutant screening. P.C.R. supervised the work and provided funding and resources. J.C.-Y.L. wrote and revised the manuscript with edits from P.C.R.

References

1. Ogawa-Ohnishi, M. *et al.* Peptide ligand-mediated trade-off between plant growth and stress response. *Science* **378**, 175–180 (2022).

2. Wang, Y., Chen, W., Ou, Y., Zhu, Y. & Li, J. Arabidopsis ROOT ELONGATION RECEPTOR KINASES negatively regulate root growth putatively via altering cell wall remodeling gene expression. *J Integr Plant Biol* **64**, 1502–1513 (2022).

3. Ercoli, M. F., Shigenaga, A. M., Araujo, A. T. de, Jain, R. & Ronald, P. C. Tyrosine-sulfated peptide hormone induces flavonol biosynthesis to control elongation and differentiation in Arabidopsis primary root. 2024.02.02.578681 Preprint at https://doi.org/10.1101/2024.02.02.578681 (2024).

4. Yimer, H. Z. *et al.* Root-knot nematodes produce functional mimics of tyrosine-sulfated plant peptides. *Proceedings of the National Academy of Sciences* **120**, e2304612120 (2023).

5. Ercoli, M. F. *et al.* Plant immunity: Rice XA21-mediated resistance to bacterial infection. *Proc. Natl. Acad. Sci. U. S. A.* **119**, (2022).

6. Li, Q., Sapkota, M. & van der Knaap, E. Perspectives of CRISPR/Cas-mediated cis-engineering in horticulture: unlocking the neglected potential for crop improvement. *Hortic Res* **7**, 1–11 (2020).

7. Rodríguez-Leal, D., Lemmon, Z. H., Man, J., Bartlett, M. E. & Lippman, Z. B. Engineering Quantitative Trait Variation for Crop Improvement by Genome Editing. *Cell* **171**, 470-480.e8 (2017).

8. Liu, L. *et al.* Enhancing grain-yield-related traits by CRISPR–Cas9 promoter editing of maize CLE genes. *Nat. Plants* **7**, 287–294 (2021).

9. Song, X. *et al.* Targeting a gene regulatory element enhances rice grain yield by decoupling panicle number and size. *Nat Biotechnol* **40**, 1403–1411 (2022).

538 10. Duan, Y.-B. *et al.* Identification of a regulatory element responsible for salt induction
539 of rice OsRAV2 through ex situ and in situ promoter analysis. *Plant Mol Biol* **90**, 49–
540 62 (2016).

541 11. Xu, Z. *et al.* Engineering Broad-Spectrum Bacterial Blight Resistance by
542 Simultaneously Disrupting Variable TALE-Binding Elements of Multiple Susceptibility
543 Genes in Rice. *Molecular Plant* **12**, 1434–1446 (2019).

544 12. Li, C. *et al.* A new rice breeding method: CRISPR/Cas9 system editing of the Xa13
545 promoter to cultivate transgene-free bacterial blight-resistant rice. *Plant*
546 *Biotechnology Journal* **18**, 313–315 (2020).

547 13. Oliva, R. *et al.* Broad-spectrum resistance to bacterial blight in rice using genome
548 editing. *Nat Biotechnol* **37**, 1344–1350 (2019).

549 14. Holme, I. B. *et al.* Evaluation of the mature grain phytase candidate HvPAPhy_a
550 gene in barley (Hordeum vulgare L.) using CRISPR/Cas9 and TALENs. *Plant Mol Biol*
551 **95**, 111–121 (2017).

552 15. Jia, H., Orbović, V. & Wang, N. CRISPR-LbCas12a-mediated modification of citrus.
553 *Plant Biotechnology Journal* **17**, 1928–1937 (2019).

554 16. Jia, H., Orbovic, V., Jones, J. B. & Wang, N. Modification of the PthA4 effector
555 binding elements in Type I CsLOB1 promoter using Cas9/sgRNA to produce
556 transgenic Duncan grapefruit alleviating XccΔpthA4:dCsLOB1.3 infection. *Plant*
557 *Biotechnology Journal* **14**, 1291–1301 (2016).

558 17. Peng, A. *et al.* Engineering canker-resistant plants through CRISPR/Cas9-targeted
559 editing of the susceptibility gene CsLOB1 promoter in citrus. *Plant Biotechnol. J.* **15**,
560 1509–1519 (2017).

561 18. Li, T. *et al.* Domestication of wild tomato is accelerated by genome editing. *Nat*
562 *Biotechnol* **36**, 1160–1163 (2018).

563 19. Li, X. *et al.* Programmable base editing of mutated TERT promoter inhibits brain
564 tumour growth. *Nat Cell Biol* **22**, 282–288 (2020).

565 20. O'Malley, R. C. *et al.* Cistrome and Epicistrome Features Shape the Regulatory DNA
566 Landscape. *Cell* **165**, 1280–1292 (2016).

567 21. Wendrich, J. R. *et al.* Vascular transcription factors guide plant epidermal responses
568 to limiting phosphate conditions. *Science* **370**, eaay4970 (2020).

569 22. Wan, J. *et al.* MYB70 modulates seed germination and root system development in
570 Arabidopsis. *iScience* **24**, 103228 (2021).

571 23. Rashotte, A. M. *et al.* A subset of Arabidopsis AP2 transcription factors mediates
572 cytokinin responses in concert with a two-component pathway. *Proceedings of the*
573 *National Academy of Sciences* **103**, 11081–11085 (2006).

574 24. Shi, J. *et al.* ARGOS8 variants generated by CRISPR-Cas9 improve maize grain
575 yield under field drought stress conditions. *Plant Biotechnology Journal* **15**, 207–216
576 (2017).

577 25. Gaudinier, A., Tang, M., Bågman, A.-M. & Brady, S. M. Identification of Protein–DNA
578 Interactions Using Enhanced Yeast One-Hybrid Assays and a Semiautomated
579 Approach. in *Plant Genomics: Methods and Protocols* (ed. Busch, W.) 187–215
580 (Springer, New York, NY, 2017). doi:10.1007/978-1-4939-7003-2_13.

581 26. Deplancke, B., Vermeirssen, V., Arda, H. E., Martinez, N. J. & Walhout, A. J. M.
582 Gateway-Compatible Yeast One-Hybrid Screens. *Cold Spring Harb Protoc* **2006**,
583 pdb.prot4590 (2006).

584 27. Gaudinier, A. *et al.* Enhanced Y1H assays for Arabidopsis. *Nat. Methods* **8**, 1053–5
585 (2011).

586 28. Pruneda-Paz, J. L. *et al.* A Genome-Scale Resource for the Functional
587 Characterization of Arabidopsis Transcription Factors. *Cell Reports* **8**, 622–632
588 (2014).

589 29. Shannon, P. *et al.* Cytoscape: A Software Environment for Integrated Models of
590 Biomolecular Interaction Networks. *Genome Res.* **13**, 2498–2504 (2003).

591 30. Lee, T. A. *et al.* A Single-Nucleus Atlas of Seed-to-Seed Development in
592 Arabidopsis. 2023.03.23.533992 Preprint at
593 https://doi.org/10.1101/2023.03.23.533992 (2023).

594 31. Nobori, T. *et al.* A rare PRIMER cell state in plant immunity. *Nature* **638**, 197–205
595 (2025).

596 32. Clough, S. J. & Bent, A. F. Floral dip: a simplified method for Agrobacterium-
597 mediated transformation of Arabidopsis thaliana. *Plant J.* **16**, 735–43 (1998).

598 33. Pound, M. P. *et al.* RootNav: Navigating Images of Complex Root Architectures.
599 *Plant Physiol* **162**, 1802–1814 (2013).

600 34. Labun, K. *et al.* CHOPCHOP v3: expanding the CRISPR web toolbox beyond
601 genome editing. *Nucleic Acids Research* **47**, W171–W174 (2019).

602 35. Xie, K., Minkenberg, B. & Yang, Y. Boosting CRISPR/Cas9 multiplex editing
603 capability with the endogenous tRNA-processing system. *Proceedings of the National*
604 *Academy of Sciences* **112**, 3570–3575 (2015).

605 36. Ursache, R., Fujita, S., Dénervaud Tendon, V. & Geldner, N. Combined fluorescent
606 seed selection and multiplex CRISPR/Cas9 assembly for fast generation of multiple
607 Arabidopsis mutants. *Plant Methods* **17**, 111 (2021).

608 37. Katagiri, F., Thilmony, R. & He, S. Y. The Arabidopsis Thaliana-Pseudomonas
609 Syringae Interaction. *Arabidopsis Book* **1**, e0039 (2002).

610

611 **Figures**

612

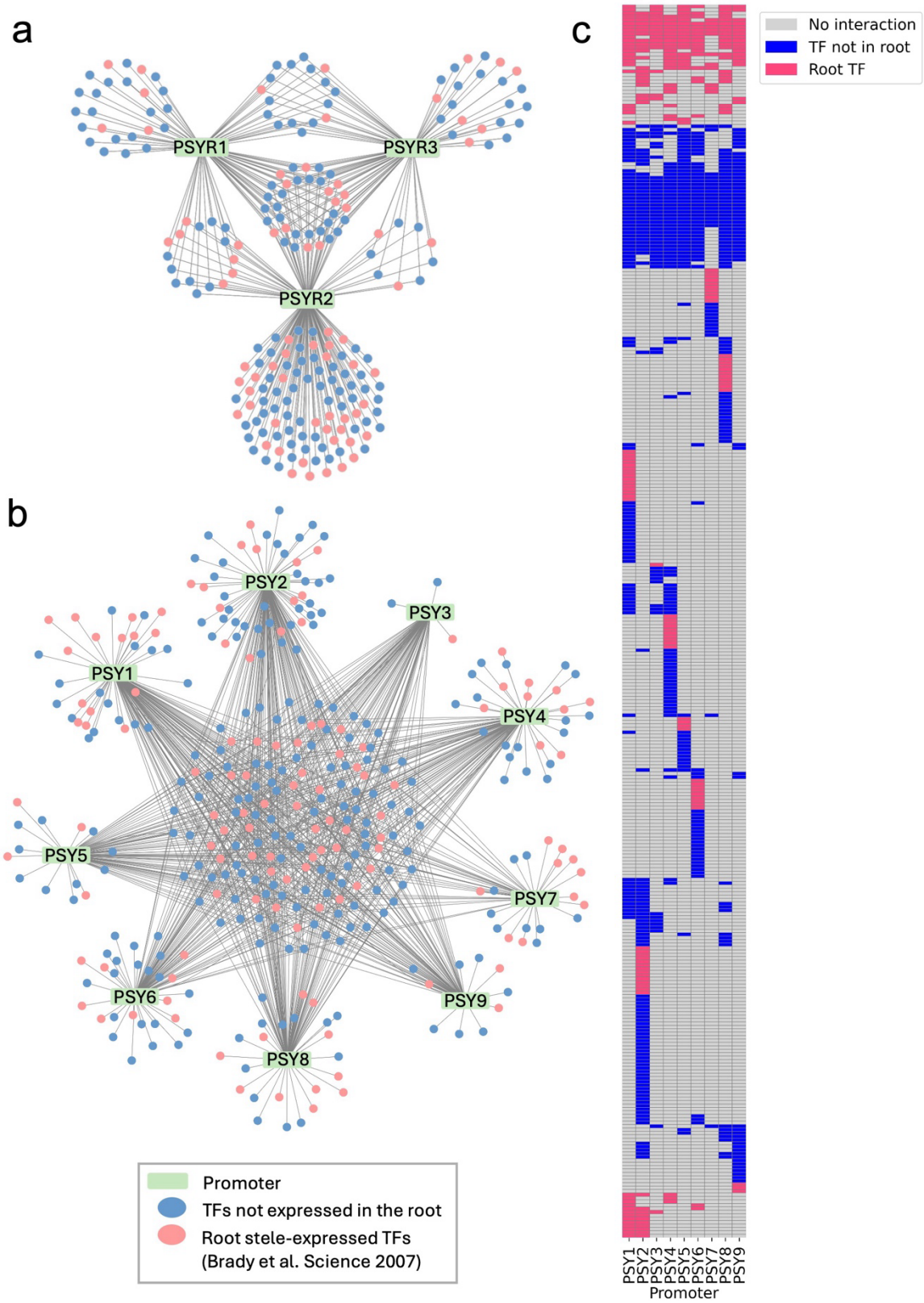

613

614 **Fig. 1. TF-*PSYR*/*PSY* promoter interaction network.**

615 **a.** TF–promoter interactions involved in PSY perception, identified by eY1H (*PSYR1*–
616 *PSYR3*, 3 promoters).
617 **b.** TF–promoter interactions involved in PSY peptide transcription, identified by eY1H
618 (*PSY1*–*PSY9*, 9 promoters). Rectangles represent promoters; small circles represent
619 TFs. Pink circles indicate root-expressed TFs (Brady et al., 2007), and blue circles
620 indicate TFs expressed in non-root tissues.
621 **c.** Heatmap of TF-promoter interactions for PSY peptide transcription identified by
622 eY1H, with shared TFs clustered. Coloring follows panel b: pink = root-expressed TFs
623 (Brady et al., 2007), blue = non-root tissues.

624

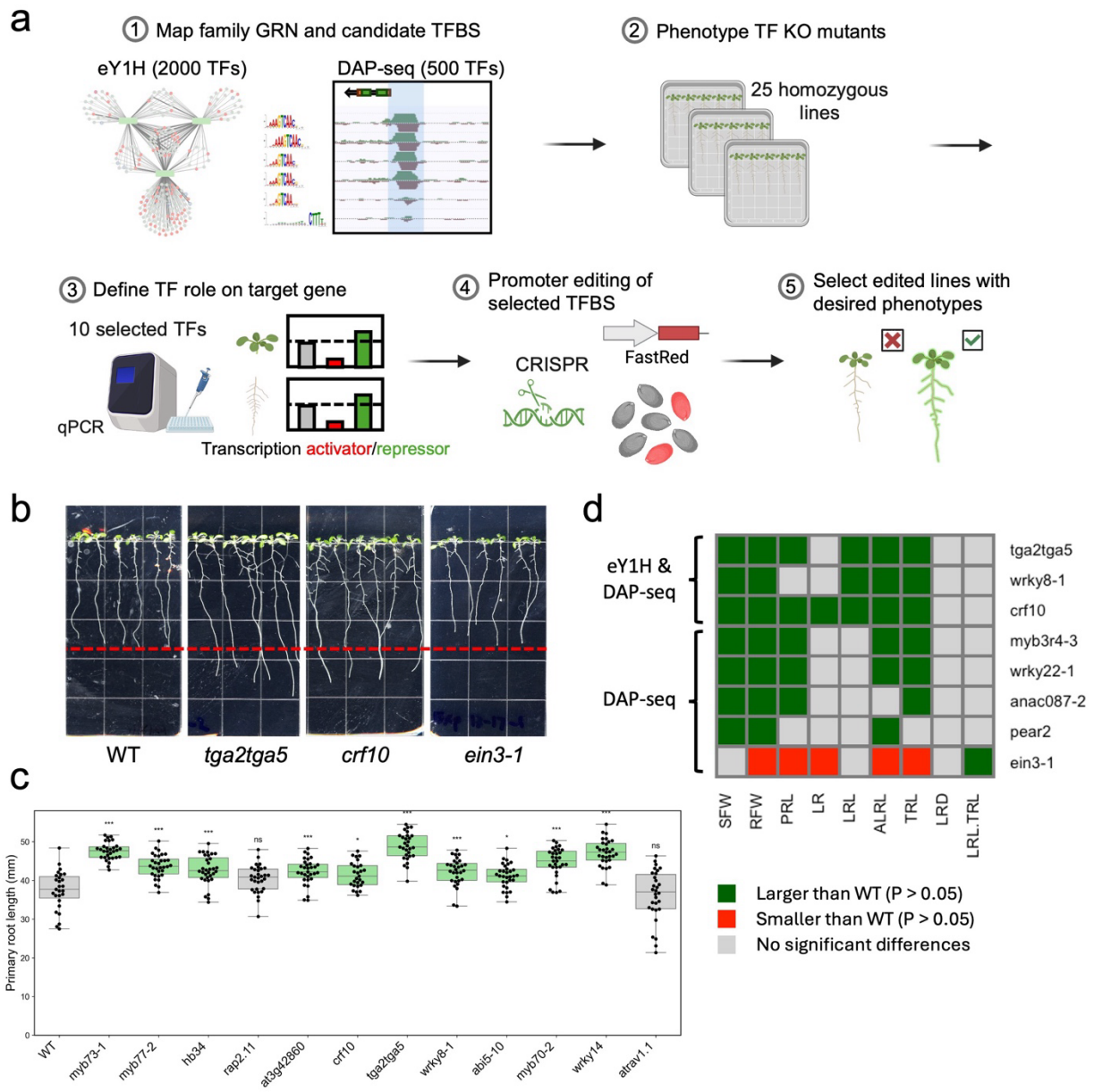

Fig. 2. Network-guided TFBS editing for precise promoter modification.
a. Schematic of the screening and editing workflow applied to *PSYR*/*PSY* promoters.
b. Representative 10-day-old TF knockout seedlings identified based on validated TF-promoter interactions. WT, Col-0.
c. Primary root length of 12 TF knockout mutants at 10 days old. Green indicates a statistically significant increase relative to WT, and grey indicates not significantly different ($P < 0.05$, one-way ANOVA; exact n and P values are in Supplementary Data 3).
d. Heatmap showing phenotypes associated with TF knockout alleles. Selected mutant alleles, identified from both eY1H and DAP-seq or from DAP-seq only, are listed in rows,

636 and measured traits are shown in columns. Statistically significant differences relative to
637 WT are indicated by colored cells ($P < 0.05$, one-way ANOVA; exact n and P values are
638 in Supplementary Data 3). From left to right, traits include shoot fresh weight (SFW, g
639 per 10 seedlings), root fresh weight (RFW, g per 10 seedlings), primary root length
640 (PRL, mm), number of lateral roots (LR), total lateral root length (LRL, mm), total root
641 length (TRL, PRL + LRL, mm), average lateral root length (ALRL, LRL ÷ LR, mm),
642 lateral root density (LRD, LR ÷ PRL), and proportion of total root length contributed by
643 lateral roots (LRL ÷ TRL). Root traits were measured from 10-day-old seedlings. Green
644 indicates a statistically significant increase relative to WT, red indicates a statistically
645 significant decrease, and grey indicates not significantly different from WT ($P < 0.05$,
646 one-way ANOVA).

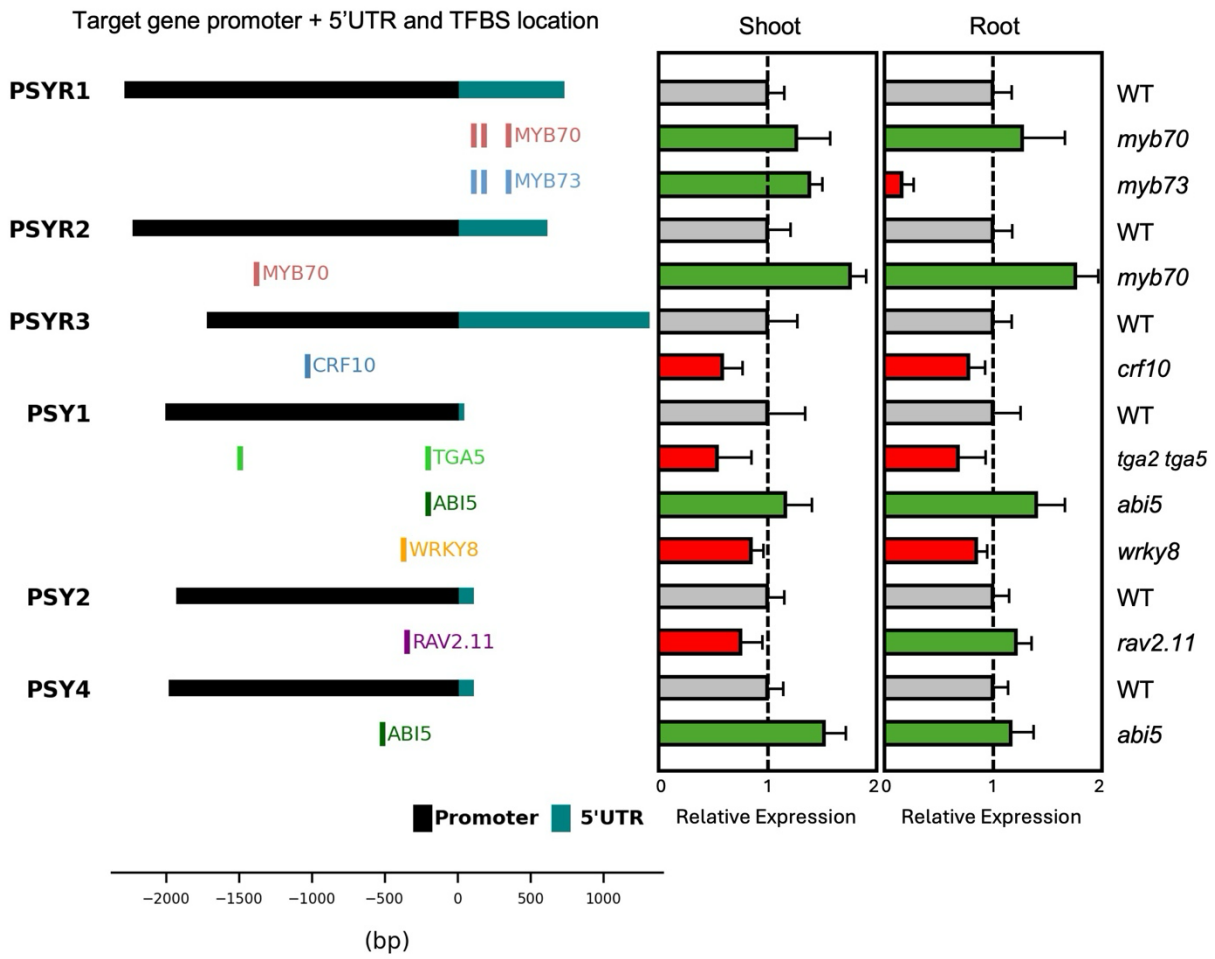

Fig. 3. Tissue-specific transcriptional changes in TF knockout mutants.

Expression of targeted *PSYR*/*PSY* genes in seedling shoots and roots of 10-day-old TF knockout seedlings. Left, schematic of target *PSYR*/*PSY* promoters and 5'UTR showing the locations of transcription factor binding sites (TFBS) validated via DAP-seq. Right, relative expression of target *PSYR*/*PSY* genes in TF knockout seedlings. For each biological replicate, 10 shoots or 20 roots were pooled. Gene expression was measured by qPCR, with WT normalized to 1 (grey bars). Expression levels significantly increased or decreased in the TF knockout relative to WT are indicated in green (TF is a transcriptional repressor) or red (TF is a transcriptional activator), respectively. Values represent mean ± SD (n = 3 biological replicates); exact *P* values are reported in Supplementary Data 4.

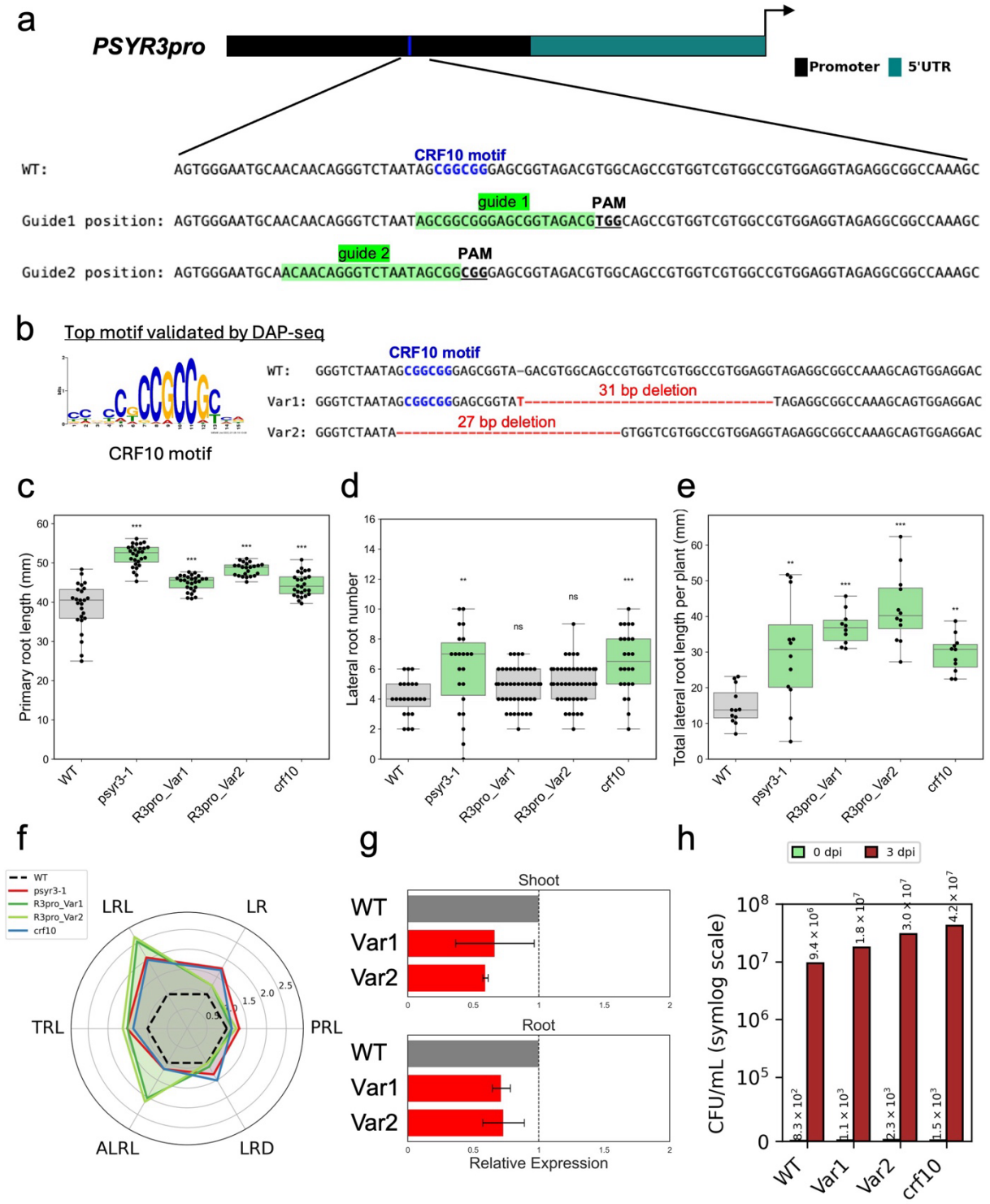

Fig. 4. CRF10 motif editing in the *PSYR3* promoter boosts root growth and *Pst* DC3000 resistance.

a. Schematic of the *PSYR3* promoter showing the CRF10 motif targeted for deletion. **b.** DNA sequence comparison of two promoter-edited variants (Var1 and Var2) relative

666 to WT. Deleted CRF10 motifs are highlighted in red; dashes indicate deleted
667 nucleotides.
668 **c-f.** Root traits measured in 10-day-old seedlings.
669 **c.** Primary root length of WT, *psyr3-1*, *crf10*, and promoter-edited plants. Boxplots show
670 median, interquartile range, and full range.
671 **d.** Number of visible lateral roots per genotype.
672 **e.** Total lateral root length per genotype.
673 **f.** Radar plot comparing root traits across genotypes: PRL, primary root length (mm);
674 LR, number of lateral roots; LRL, total lateral root length (mm); ALRL, average lateral
675 root length (LRL ÷ LR, mm); TRL, total root length (PRL + LRL, mm); LRD, lateral root
676 density (LR ÷ PRL).
677 **g.** *PSYR3* expression in shoot and root tissues of 10-day-old promoter-edited seedlings.
678 Values represent mean ± SD (n = 3 biological replicates); exact *P* values are reported in
679 Supplementary Data 4.
680 **h.** *Pseudomonas syringae* pv. *tomato* DC3000 accumulation in promoter-edited variants
681 versus *crf10*. Bacteria were infiltrated into 4-week-old plants, and leaf discs were
682 collected at different days post-infiltration (dpi). CFUs per leaf disc were measured;
683 averages ± SD from three replicates are shown. Experiments were repeated more than
684 three times with similar results.

685

686 **Supplemental Materials**

687 All supplemental materials referenced in the text will be provided in the final published
688 version. All main findings are fully presented in the figures included in this manuscript.

689

690 **Supplementary Figures**

691

692 **Supplementary Fig. 1. Overlap of eY1H and DAP-seq interactions.**
693 Venn diagram showing TFs identified by either eY1H or DAP-seq for three *PSYR*
694 promoters and nine *PSY* promoters. Yellow circle indicates TFs identified by eY1H, and
695 blue circle indicates TFs identified by DAP-seq.

696 **Supplementary Fig. 2. *PSYR*/*PSY* expression at the whole plant level.**
697 Data were extracted from the public available bulk RNA-seq database.

698 **Supplementary Fig. 3. *PSYR*/*PSY* expression at the single-cell level in roots.**
699 Data were extracted from the Plant sc-Atlas database.

Supplementary Fig. 4. Co-expression patterns between candidate TFs and their target PSYR/PSY genes.
Heatmaps show co-expression relationships for selected TF–target pairs.

Supplementary Fig. 5. Confirmation of selected TF knockouts.
qPCR analysis of selected TF expression in TF knockout (KO) mutants. Gene expression was measured by qPCR and normalized to wild-type (WT = 1, grey bars). Expression levels showing a significant decrease are indicated in red. Values represent mean ± SD (n = 3 biological replicates); exact *P* values are reported in Supplementary Data 4.

Supplementary Fig. 6. Comparison of primary root length in selected Arabidopsis mutant alleles of transcription factors identified by DAP-seq.
Primary root length of 10 TF KO mutants at 10 days old. Exact *P* values are reported in Supplementary Data 3.

Supplementary Fig. 7. CRF10 is a strong growth repressor.
Overexpression of CRF10 causes an extreme dwarf phenotype. Forty-day-old adult plants are shown. Scale bar = 1 cm.

Supplementary Datasets

Supplementary Dataset 1. List of eY1H results.

Supplementary Dataset 2. Overlap of eY1H and DAP-seq interactions.

Supplementary Dataset 3. RSA (root system architecture) phenotyping data.

Supplementary Dataset 4. qPCR gene expression data.

Supplementary Tables

Supplementary Table 1. Genotyping, qPCR, and cloning primers.

Supplementary Table 2. Summary of mutants, transgenic plants, and promoter-edited plants.